Multiscale and Multidisciplinary Modeling, Experiments and Design (2025) 8:64
https://doi.org/10.1007/s41939-024-00663-5

ORIGINAL PAPER

Predicting brain tumor presence using machine learning models

Weiguo Huang[1] · **Zhenhua Dai**[1]

Received: 29 May 2024 / Accepted: 3 November 2024 / Published online: 17 November 2024

Abstract
A brain tumor is an abnormal growth of the cells within the brain either benign or malignant. The benign ones have relatively slow growth and do not contain any cancerous component, whereas the malignant ones are dangerous as they contain cancerous tendencies and grow at very high rates, extending into the surrounding tissue of the brain. The signs and symptoms of brain tumors depend on position and size but may involve seizures, headaches, abnormalities in vision or hearing, problems in cognition, and inefficient body movements. The diagnosis is usually made by imaging studies such as MRI or CT scan, and the management may be chemotherapy, surgery, radiation therapy, or a combination. The hallmark of improved prognosis in brain tumors is early diagnosis and treatment. The prediction of brain tumors using Machine Learning models like the Extreme Learning Model (ELM) and Decision Tree Classification is done by strategically implementing 2 sophisticated optimizers known as the Mayfly Optimizer and Flying Fox Optimization algorithm. These have contributed to increasing the inherent accuracy of the models. In turn, this leads to the emergence of these models, together with the optimizers, into a synergistic whole that causes a remarkable increase in the accuracy of prediction. In particular, during training, the DTFF model is far ahead among its competitors, providing very impressive accuracy of 0.951, unparalleled by any other model. Then comes the DTMO model, being the runner-up, with an accuracy of 0.932. Conversely, the ELM model, with an accuracy of 0.824, falls short of demonstrating robust predictive capabilities, underscoring its limitations within the prediction process.

Keywords Extreme learning model · Decision tree classification · Brain tumor · Mayfly optimizer · Flying fox optimization algorithm

1 Introduction

A brain tumor is an abnormal proliferation of cells in the brain. These growths might be benign (not cancerous) or malignant (cancerous). They originate when normal cells have genetic abnormalities, leading them to grow uncontrolled and form a mass or tumor inside the brain tissue. Brain tumors can develop from inside the brain (primary tumors) or spread from other regions of the body (metastatic tumors) (Cacho-Díaz et al. 2020). The symptoms of a brain tumor differ based on its location, size, and kind, but frequent indicators include speech difficulty, headaches, visual problems, seizures, and movement dysfunction (Pekmezci and Perry 2013). For conclusive categorization, diagnostic procedures that include CT (Computed Tomography) or MRI (Magnetic Resonance Imaging) scans are usually utilized in conjunction with neurological evaluations and, in certain cases, a biopsy (Abd-Ellah et al. 2019; Shankar et al. 2017). Brain tumors can be treated with surgery, radiation treatment, chemotherapy, targeted medication therapy, or both of these methods (Park et al. 2021). The kind and location of the tumor, its size, and the patient's general health all influence therapy decisions. Early identification and timely action are critical for controlling brain tumors and improving patient outcomes.

Brain tumors can cause a variety of neurological symptoms, including chronic headaches, cognitive impairment, and seizures (Ghandour et al. 2021). Headaches caused by brain tumors are generally strong and frequent, and they might intensify with time, especially in the morning or with changes in posture (Hadidchi et al. 2019). Seizures can take many forms depending on where the tumor is located, such as focal seizures to widespread tonic–clonic seizures (Bauer et al. 2014). Furthermore, neurological abnormalities such as paralysis, numbness, speech difficulty, and visual changes may result from the tumor's compression or invasion of neighboring brain tissue (Robert-Boire et al. 2019).

✉ Zhenhua Dai
17769348262@163.com

[1] School of Information Engineering, Hunan University of Science and Engineering, Yongzhou 425199, Hunan, China

Memory issues, confusion, and personality changes are all possible cognitive changes that can influence a person's daily functioning as well as quality of life (Durand et al. 2018; Lemaitre et al. 2021). In addition, brain tumors can cause nausea, vomiting, and exhaustion, which complicates the clinical picture. Visual abnormalities, motor limitations, and behavioral changes are other symptoms that may appear depending on the tumor's location and size (Gordon et al. 2014; Woroniecka et al. 2018). As the tumor develops, symptoms often increase, emphasizing the necessity of early discovery and action for successful therapy and a better prognosis (Batta 2017).

Brain tumors are often divided into 4 stages, known as grades, depending on their appearance under a microscope and aggressiveness.

Grade I: These tumors are the least dangerous and are commonly referred to as benign tumors. They develop slowly and have well-defined edges, much like normal cells under a microscope. Grade I tumors are frequently treatable with surgery alone, and they seldom return after removal (Thust et al. 2018).

Grade II: These tumors are classified as low-grade and exhibit somewhat more aggressive activity than Grade I tumors. They may develop faster and have less defined bounds. While they remain generally slow-growing, Grade II tumors are more likely to return and may need further treatments that involve chemotherapy or radiation therapy following surgical resection.

Grade III: These tumors, known as high-grade or anaplastic tumors, are more aggressive than Grade II tumors. They develop quickly and have unusual-looking cells under a microscope. Grade III cancers frequently penetrate neighboring neural tissue and have a greater probability of recurrence, even after vigorous therapy (Sudha et al. 2014).

Grade IV: These are the most dangerous tumors, known as glioblastomas. They develop quickly, penetrate the surrounding brain tissue heavily, and contain extremely aberrant cells under a microscope. Grade IV tumors are difficult to treat and have a dismal prediction, with a median lifespan of only 12–15 months with vigorous therapy (Priya et al. 2016).

Each grade signifies a distinct amount of malignancy and aggressiveness, which influences treatment options and prognosis for people with brain tumors.

ML algorithms may forecast brain cancers by evaluating multiple forms of medical imaging data, including CT, MRI, as well as PET (Positron Emission Tomography) images. These algorithms employ powerful algorithms for pattern recognition to detect tiny irregularities in pictures that might signal the presence of a tumor (Alzubi et al. 2019). Trained on large datasets consisting of images with their labels, an ML algorithm may learn to differentiate between normal brain tissue and different types of tumors. Similarly, tumors can be classified based on their locations, shapes, and sizes (Bakas et al. 2018).

These include texture, intensity, and geometric features extracted from the imaging data and are fed into the ML model. Consequently, such features allow the ML algorithm to learn patterns regarding tumor presence. ML can be very helpful in segmenting tumors, a process whereby the borders of a tumor are outlined in images obtained from imaging. It can also combine different types of imaging and clinical data in machine learning algorithms to reach a higher diagnostic precision that will help the physicians make more informed decisions on the treatment of the patients (Zhou et al. 2018). Hence, ML becomes the strong tool for the early identification, characterization, and management of brain tumors that can lighten the burden on healthcare systems and improve outcomes among patients.

1.1 Descriptive epidemiology

Between 1998 and 2002, the average yearly incidence of incident (newly diagnosed) primary brain tumors in the United States was 14.4 per 100,000 persons (Dolecek et al. 2012). Over time, the number of brain tumors has increased as well as varies depending on the area, gender, age, and race. Based on nine regions assessed by the US SEER program from 1973, the age-adjusted incidence rate of malignant brain tumors has increased (from 4.1 per 100,000 women in 1973 to 5.2 per 100,000 women in 2003) in both men and women, rising from 5.9 per 100,000 in 1973 to 7.0 per 100,000 in 2003. The majority of the rise in instances can probably be attributed to improvements in diagnostic imaging, notably the application of MRI and CT scans, increased access to a wider range of medical care and neurosurgeons, modifications to treatment protocols for elderly patients, and adjustments to the categorization of certain histologies of brain tumors (Wrensch et al. 2002). Age-adjusted average annual prevalence rate (1998–2002) for females (15.1 per 100,000 person-years) for all central nervous system (CNS) malignancies (brain tumors being the majority) is somewhat higher than that of males (14.5 per 100,000 person-years). For the main histologic groupings and a few frequent histological subtypes of brain tumors, Table 1 shows the average yearly age-adjusted rates of incidence and median ages of detection for the years 1997 to 2001. Table 1 shows that men are more likely to develop glioma and germ cell tumors, whereas women are almost twice as likely to develop meningiomas. The gender gap is almost four times greater among Polynesians (Olson and Law 2005). Between 1998 and 2002, the mean age of diagnosis for all patients in the United States with a primary brain tumor was 57 years old (Dolecek et al. 2012).

Table 1 Annual prevalence rates of primary brain tumors (main histologic groups and chosen subtypes) by gender during 1998–2002, including the age-adjusted, median ages at diagnosis, and number of cases averages

Histologic group	Number of cases	Median age at diagnosis (years)	Rate	Male Rate	Female rate
Tumors of neuroepithelial tissue/glioma	27,776	53	6.42	7.67	5.35
Pilocytic astrosytoma	1465	12	0.33	0.34	0.32
Diffuse astrocytoma	428	46	0.10	0.11	0.08
Anaplastic astrosytoma	2029	51	0.47	0.56	0.38
Glioblastoma	12,943	64	3.05	3.86	2.39
Oligodentoglioma	1559	41	0.35	0.38	0.33
Anaplastic oligodentoglioma	781	48	0.18	0.20	0.16
Ependymoma/anaplastic	1126	39	0.26	0.29	0.22
Mixed glioma	722	42	0.16	0.19	0.14
Malignant glioma, not else specified	1668	43	0.38	0.42	0.35
Benign and malignant neuronal/glial, neuronal and mixed	944	26	0.21	0.23	0.19
Embryonal/primitive/medulloblastoma	1094	9	0.24	0.29	0.19
Tumors of meninges	19,980	63	4.70	2.95	6.16
Germ cell tumors	397	17	0.09	0.12	0.06
Menangiom	19,190	64	4.52	2.75	6.01
Tumores of sellar region	4496	48	1.03	1.05	1.03

The rates are per 100,000 population, age-adjusted to the 200 United States (19 age groups) standard, and are according to cancer incident data from the following registries: Colorado, Arizona, Delaware, Connecticut, Maine, Idaho, Massachusetts, Montana, Minnesota, New York, North Carolina, New Mexico, Texas, Virginia, Utah. Primary brain tumors in the United States, 1998–2002, from the CBTRUS statical report

1.2 Objectives

The primary objective of this research is to utilize advanced ML techniques to forecast brain tumors. The study employs sophisticated models such as DTC and ELM, which are fine-tuned using the MO and the FFO algorithms to maximize their predictive capabilities. The DTC is chosen as a baseline due to its simplicity and interpretability, providing a clear comparison against optimized models. ELM is selected for its rapid learning speed and effectiveness in handling large datasets, making it suitable for complex tasks like brain tumor prediction. MO is valued for its balance between exploration and exploitation, while FFO's ability to avoid local minima drives a more precise and globally optimal solution. These will be integrated with optimization algorithms to develop hybrid models, which give higher accuracy in predicting brain tumors. Similarly, the developed hybrid models are rigorously evaluated and compared for tumor and nontumor conditions by generating comprehensive plots and tables, thus enabling detailed analysis to be performed. This systematic evaluation methodology will be used in the proposed research in an attempt to decide on the most effective model to accurately predict brain tumors under different conditions. Comparison of the results from different models will help give useful insights into the optimum approach for precise brain tumor prediction using ML methodologies.

2 Material and models

2.1 Data collection

The primary objective of this research is to utilize advanced ML techniques to forecast brain tumors. To achieve this goal, a dataset that contains 3762 samples extracted from the previous study (Brain Tumor Data n.d.), is utilized. This dataset includes five first-order characteristics and eight texture attributes at the target level:

- Initial Features Mean: Variance, Standard Deviation, Skewness, and Kurtosis.
- Second Order Features: Contrast, Energy, ASM (Angular second moment), Entropy, Homogeneity, Dissimilarity, Correlation, and Coarseness.

The preprocessing stage included applying random permutation (randperm) to reduce biases and normalization techniques to standardize the parameter scales, enhancing the dataset's suitability for analysis. Also, by implementing the Variance Inflation Factor (VIF), which is considered one of the feature selection methods, the most critical features can be discovered for conducting research.

The VIF can be used for the identification of variables in a dataset that are highly correlated with others. If the

Table 2 Description of features and determination of selected features

No	Feature	VIF score-initial feature vector	VIF score-reduced feature vector
1	Mean	27.59464	2.277464
2	Variance	104.2748	Removed
3	Standard Deviation	361.9863	Removed
4	Entropy	18,400.78	Removed
5	Skewness	87.32174	7.01178
6	Kurtosis	14.95906	3.605921
7	Contrast	13.63883	2.861284
8	Energy	756.3902	Removed
9	ASM	13,180	1.726275
10	Homogeneity	362.4068	Removed
11	Dissimilarity	86.13957	Removed

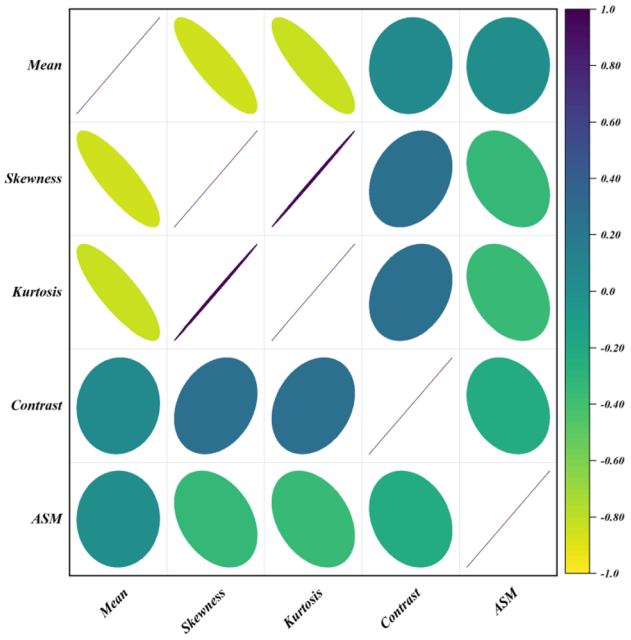

Fig. 1 Correlation matrix for the relations of the input and output

VIF value is high, it states that there is some problem with the multicollinearity among regressors. Probably the most usual strategy for dealing with it is the systematic removal of regressors based on VIF ranking. VIF scores iteratively drop for the remaining variables as each is removed according to VIF ranking, starting with the highest-scoring variable. Generally, VIF scores between 5 and 10 are considered acceptable, with this study using a threshold of 10. The iterative method continues removing the variable with the highest VIF score, recalculating the scores for the remaining variables until all variables fall below the threshold of 10. Table 2 summarizes the results of applying the VIF method in this study. It reveals that features such as standard deviation, entropy, variance, energy, homogeneity, and dissimilarity were excluded due to their VIF scores exceeding 10. In the end, features like mean, skewness, kurtosis, contrast, and ASM were retained for further analysis.

Following the identification of the most influential features, a correlation analysis was performed to assess the impact of each feature on the outputs and their relationships with other features. This analysis is illustrated in Fig. 1. Based on Fig. 1, the features of mean and contrast have the most significant influence on brain tumor prediction. Additionally, kurtosis and skewness demonstrate a strong correlation with each other, as do skewness and contrast. Further specifics can be found in the referenced figure.

2.2 Extreme learning model (ELM)

For both classification and regression applications, an ELM is a concealed-layer feed-forward neural network (SLFN) based on least squares (Pal and Deswal 2014). Huang et al. (Huang et al. 2011) in ELM structure, a kernel function was employed instead of a hidden layer with an abundance of nodes. Pal and Deswal (Pal and Deswal 2014) and Huang et al. (Huang et al. 2011) the 2 recommended techniques are outlined below. The ELM with hidden neurons, H, training data, N, as well as activation function $f(x)$ is as follows:

$$e_j = \sum_{i=1}^{H} \alpha_i f(w_i, c_i, x_i) j = 1, \ldots, N \tag{1}$$

The input-hidden and hidden-output layers are indicated by the weight vectors w_i and α_i in that order. The input parameters are denoted by x_i. The hidden bias of the ith hidden neuron is represented by c_i, while the ELM output for data point j is represented by e_j. The input weights are created at random as well as have an ongoing probability distribution (Pal and Deswal 2014). The final values are obtained using a linear Eq. (2), which may be simplified as follows:

$$\beta = A\dagger Y \tag{2}$$

Equation (3) includes the hidden layer's output matrix (A), ELM target values (Y), its Moore–Penrose modified inverse ($A\dagger$). Equation (2) may be written to $A\alpha = Y$, where A represents the neural network's hidden layer output matrix and Y represents the output parameter vectors. The 3 matrices

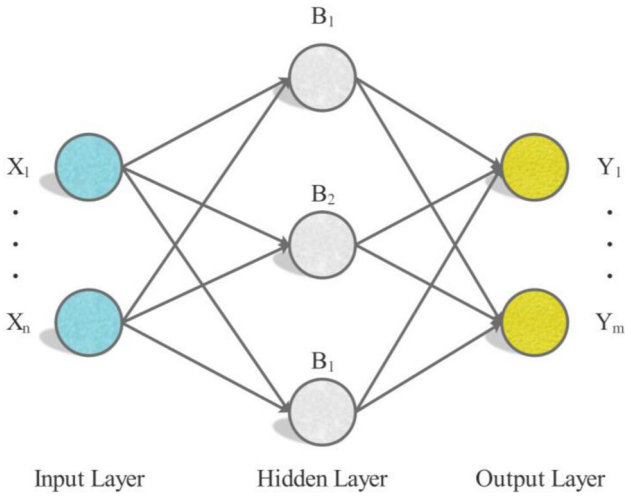

Fig. 2 The ELM is a feed-forward neural network with a single hidden layer

in a compact arrangement are expressed as follows:

$$A = \begin{bmatrix} h(x_1) \\ \vdots \\ h(x_n) \end{bmatrix} = \begin{bmatrix} f(w_1, c_1, x_1) \ldots f(w_H, c_H, x_i) \\ \vdots \\ f(w_1, c_1, x_j) \ldots f(w_H, c_H, x_j) \end{bmatrix},$$
$$\alpha = \begin{bmatrix} \alpha_1^T \\ \vdots \\ \alpha_H^T \end{bmatrix}, \; and Y = \begin{bmatrix} y_1^T \\ \vdots \\ y_N^T \end{bmatrix} \tag{3}$$

$h(x)$ is the hidden layer's feature mapping. The ELM method's output is primarily dependent on matrix A. When utilizing the standard technique, the hidden layer makes use of the neural network, as well as optimization using gradient-based algorithms can be used to solve matrix A, as given in Pal and Deswal (2014). Next, the ELM is solved using the kernel $k(x_i x_j)$ function, and the kernel matrix can be computed using feature mapping in the manner shown below (Pal and Deswal 2014; Huang et al. 2011; Naji 2018):

$$k = (x_i, x_j) = h(x_i) \cdot h(x_j) \tag{4}$$

In this research, ELM was used to examine the kernel's impact on the M_r the forecasting. To create a unique model for M_r forecasting for stable base aggregates, ELM was linked with PSO. The ELM outperforms typical neural connections in terms of learning rate, generalization capacity, and prediction accuracy. Basic ELM produces input weights and hidden biases at random and as well as utilizes the Moore–Penrose extended inverse technique to calculate output layer weights (Cao et al. 2012; Huang et al. 2006). Figure 2 depicts the SLFN with input layer neurons 'n', concealed layer brain cells, and output layer neurons. For instance, if the initial data is $\{X_i, Y_i\}$, then the input dataset is $X_i = [X_{i1}, X_{i2}, \ldots, X_{iN}]$, as well as the result dataset is $Y_i = [Y_{i1}, Y_{i2}, \ldots, Y_{iM}]$ and $i = 1, 2, \ldots, n.m$ is the training samples number.

2.3 Decision tree classification (DTC)

DT learning employs a DT as a prediction model to connect data regarding an object to judgments about its intended value. The DT algorithm is an information induction approach that partitions a dataset of records iteratively using either a depth-first aggressive or breadth-first strategy until all data items are assigned to a certain class.

A DT contains 3 sorts of nodes: leaf, root, and internal. It features a flowchart-like tree structure, with the top node serving as the root, each internal node representing a test condition derived from an attribute, each branch representing the result of the test condition, and each leaf node (or terminal node) identified by a class. The DT is constructed using a divide-and-conquer technique, with each path in the tree reflecting a decision rule. Overall, it requires a greedy mindset from the highest to the bottom. The DTC consists of 2 stages: tree creation and tree pruning. The tree is created from the top down, using repeated partitioning until all data items have the same class label. This method is computationally intensive since it involves many traversals of the training dataset. Tree pruning, on the other hand, starts at the bottom and works its way up to enhance the method's forecasting and categorization accuracy by decreasing overfitting. Overfitting in DT models can lead to misclassification errors. Several DT-based computations, such as ID3, C4.5, C5.0, CART, and others, supply advantages such as strong learning capabilities, rapid classification, and ease of implementation.

2.4 Mayfly optimizer algorithm

The MO mechanism would distinguish between male and female mayflies in groups (Amudha et al. 2021). Male mayflies are always stronger, which allows them to achieve more success in optimization. Members in the MO algorithm, like those in swarms of the PSO method, would adjust their locations depending on their current positions $p_i(t)$ and velocity $v_i(t)$ at the present cycle.

$$p_i(t+1) = p_i(t) + v_i(t+1) \tag{5}$$

All male and female mayflies would use Eq. (5) to update their locations. Nevertheless, the speed would be adjusted in various ways.

2.4.1 Movements of male mayflies

Male mayflies in swarms would continue their exploration or exploitation procedures throughout iterations. The velocity would be adjusted based on their present fitness values $f(x_i)$ and the historical greatest fitness levels in trajectories $f(x_{hi})$. If $f(x_i) > f(x_{hi})$, the male mayflies will adjust their velocities based on their current velocities, the distance that exists between them and the world's best location, and the previous best paths:

$$v_i(t+1) = g.v_i(t) + \alpha_i e^{-\beta r_p^2}[x_{hi} - x_i(t)] + \alpha_2 e^{\beta r_g^2}\left[x_g - x_i(t)\right] \quad (6)$$

g is a parameter that decreased linearly from its highest value to a lesser one. 2 variables (a_1, a_2, and β) are used to balance values. r_p and r_g are 2 variables used to calculate the Cartesian distance between individuals and their historical optimum position, as well as the global best position in swarms. Cartesian distance could serve as the subsequent norm for the distance vector.

$$||x_i - x_j|| = \sqrt{\sum_{k=1}^{n}\left(x_{ik} - x_{jk}\right)^2} \quad (7)$$

If $f(x_i) < f(x_{hi})$, male mayflies will change their present speeds with a random dance factor d.

$$v_i(t+1) = g.v_i(t) + d \cdot r_1 \quad (8)$$

2.4.2 Movements of female mayflies

Mayflies that are females would alter their speed. Because they can only survive for 1–7 days in the wild, female mayflies would be eager to find males in order to propagate and mate. As a result, their speeds would change depending on which male mayflies they wanted to mate with. The top male and female mayflies are treated as the first mates by the MO algorithm, which then selects the second-best male and female mayflies, and so forth. As for the i-th female mayfly, if $f(y_i) < f(x_i)$:

$$v_i(t+1) = g.v_i(t) + \alpha_3 e^{-\beta r_{mf}^2}[x_i(t) - y_i(t)] \quad (9)$$

α_3 in Eq. (9), is a constant that balances the speeds. The Cartesian distance between them is displayed by r_m. If $(y_i) < f(x_i)$, female mayflies will update their current speeds using a different randomized dance fl.

$$v_i(t) = g \cdot v_i(t) + fl \cdot r_2 \quad (10)$$

In Eq. (10) r_2 is similarly, a random integer with a consistent distribution in the domain, $[-1, 1]$.

$$offspring1 = L \times male + (1 - L) \times female$$

$$offspring2 = L \times female + (1 - L) \times male \quad (11)$$

L are selected at random from the distribution known as the Gaussian.

2.5 Flying foxes optimization (FFO)

The based population's stochastic method known as diverse approaches informs FFO, which is used by flying foxes to deal with increased temperatures (Aalloul et al. 2023). This technique uses a hybrid algorithm framework that incorporates operators from current methods (Li et al. 2023; Liu et al. 2021). The choice of population size (N), substitution list (RL), and attraction constant (b) all have a major impact on FFO performance. The stages detailed in the FFO method are as follows.

2.5.1 Flying foxes algorithm operation

Flying foxes, large bats with little echolocation, return to their homes after meals, choosing more magnificent trees; overcrowding usually leads to fatality (Kumar et al. 2021).

2.5.2 The application of FFO algorithm

A novel approach begins by picking starting points according to the flight movements of foxes, which are expressed as vectors (x) in a space with multiple dimensions. The proposed solutions at these sites are then assessed by employing an objective function. The flying foxes' mission is to find a tree with a lower temperature and survive in high-heat situations.

2.5.3 Movement of flying foxes

Given that flying foxes either follow their contemporaries' travels or seek out the next available tree, if the habitat tree does not provide the necessary lowest temperature comfort, it is acceptable to expect, that the flying foxes would relocate to another area to avoid the unbearable heat. This maneuver can be expressed numerically as follows:

$$x_{i,j}^{t+1} = x_{i,j}^{t} + a.rand(cool_j - x_{i,j}^{t}) \quad (12)$$

$x_i^0 \sim U(x_{min}, x_{max})$, $x_{i,j}^t$ indicates the $j-th$ constituent within $FF(i)$ at repetition t, where an excess a continuous, $rand \sim U(0,1)$, as well as $cool$ shows the position of the FF in the tree with the lowest temperature. Equation (13) gets

into action when $|f(cool) - f(x_i)| > \frac{\delta_1}{2}$, the vector cool reflects the flying fox's optimal position, showing the best response on record. The parameter δ_1 indicates the greatest gap between 2 flying foxes considered nearby. While reaching a tree with an exceedingly appropriate temperature $|f(cool) - \leq f(x_i)|\frac{\delta_1}{2}$, to stay out of crowds, the flying fox seeks the next open place. The below equations offer a more complete description of this occurrence.

$$x_{i,j}^{t+1} = \begin{Bmatrix} nx_{i,j}^{t+1}, ifj = k \ or \ rnd_j \ \geq pa \\ x_{i,j}^{t}, otherwise \end{Bmatrix} \tag{13}$$

$rand \sim U(0,1)$ denotes a random choice, rnd_j is a random number that varies from 0 to 1, and x_{R1}^t and d x_{R2}^t represent 2 unidentified individuals from the existing population. In addition, pa denotes a constant probability. Lastly, k is chosen randomly from the full bunch {1,2, ..., m}, which is an important factor, in ensuring that at least a single aspect $nx_{i,j}^{t+1}$ is elected by $x_{i,j}^{t+1}$, therefore, the previous response stays different from the new one. An evaluation of the computed outcomes is undertaken.

2.5.4 Death and replacement flying foxes

Many factors affect flying fox survival, including high temperatures and distance from favorite trees. Replacement List offers amazing answers.

$$x_{i,j}^{t+1} = \frac{\sum_{k=1}^{n} RL_{k,j}^{t}}{n} \tag{14}$$

In the tth repetition, $RL_{k,j}^{t}$ denotes the $k - th(FF)$ on the (RL). Equation (14) is aimed to enhance the likelihood of discovering a suitable location and utilizing its full potential. Crowding can cause flying fox mortality. Before each repeat, a probability is estimated using foxes in regions with low temperatures.

$$p^D = \frac{nc - 1}{population \ \ size} \tag{15}$$

The quantity nc is substantially related to the number of FF (Flying Felines), with the optimal solution being provided by a matching goal function.

2.5.5 Crossover process

Recombination of genes joins 2 flying foxes; 2 separate parents are chosen at random, culminating in 2 descendants in a subsequent operation.

$$\begin{aligned} offspring1 &= L.R_1 + (1-1).R_2 \\ offspring2 &= L.R_2 + (1-L).R_2 \end{aligned} \tag{16}$$

R_1 and R_2 signify different persons chosen at random from the group, whereas L is a random integer ranging from 0 to 1. Figure 3 presents the flowchart of the FFO.

2.6 Performance evaluator

Several criteria are used to evaluate classifiers' performance. Accuracy, or the percentage of properly anticipated observations, is a popular term. Common metrics include recall, accuracy, and precision. Accuracy refers to overall accuracy, which includes both true negatives and positives. Unbalanced datasets can impact accuracy. Recall identifies only positives, assuming few errors. The F1 score finds a compromise between accuracy and recall, making it effective in schools with various distributions. It fixes for both true positives and false negatives. These metrics help to determine the efficacy of ML models.

Precision Precision tells us what proportion of the positive predictions that the model makes is actually true positive. A higher precision score would mean that the model has fewer false positives, and this is much more critical in clinical applications where all the positive predictions may result in unnecessary treatments or interventions.

$$\text{Precision} = \frac{\text{TP}}{\text{TP} + \text{FP}} \tag{17}$$

Recall Recall is the percentage of actual positive cases that the model puts in the positive class. Clinically, this is a very important metric since the practitioners would want to catch as many true positives through the model to avoid any missed diagnosis.

$$\text{Recall} = \text{TPR} = \frac{\text{TP}}{\text{P}} = \frac{\text{TP}}{\text{TP} + \text{FN}} \tag{18}$$

Accuracy Accuracy will give the general correctness of the model by showing how often the predictions of the model match the actual outcomes. While accuracy is useful, it may not always be the best measure in situations where there is class imbalance. It should therefore be interpreted hand in hand with Precision and Recall in order to have a full understanding of the model's performance.

$$\text{Accuracy} = \frac{\text{TP} + \text{TN}}{\text{TP} + \text{TN} + \text{FP} + \text{FN}} \tag{19}$$

F1 Score The F1 score represents the harmonic mean of Precision and Recall, providing a balanced view of the model's performance. It is particularly valuable in scenarios where there is an uneven class distribution, as it takes both false positives and false negatives into account.

$$\text{F1 score} = \frac{2 \times \text{Recall} \times \text{Precision}}{\text{Recall} + \text{Precision}} \tag{20}$$

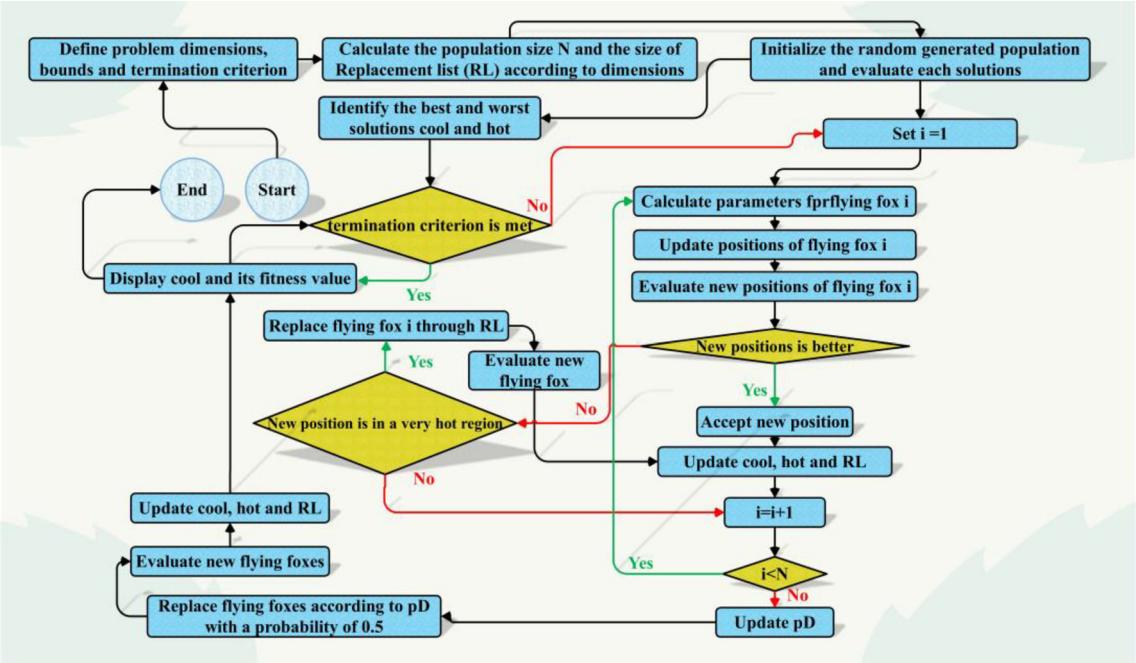

Fig. 3 The flowchart of the FFO

In each of the following calculations, the shorthand letter TP is a positive prediction of the fortunate incident. At any event and when there is an unfortunate incidence, then FP stands for positive prediction. A negative prediction as forecast from TN foretells the same as the real negative. If actual turns out to be positive then the FN is unfortunate prediction of a grim forecast.

3 Results

The results obtained from the hybrid models are analyzed in minute detail in this section. These results are presented with great care and comparative scrutiny in detail to determine which one of them offers the best functionality in the prediction process. From such a careful investigation, the model that is found to possess the highest rate of prediction accuracy and efficacy provides important insights into the performance dynamics of hybrid modeling techniques.

3.1 Hyperparameters' results

If one is going to develop machine learning models, then the systematic tuning of hyperparameters is a must in order for the models to exhibit optimum performance without any troubles associated with overfitting or excessively long times of training. The current study optimizes those hyperparameters that may be critical to both DTC and ELM models. For the DTC models, these are max_depth, min_samples_split, and min_samples_leaf, while in ELM-based models, this depends on alpha, batch_size, and density fine-tuning. The detailed values of the hyperparameters of DTC and ELM are represented in Tables 3 and 4, respectively. Besides, great care is taken for choosing and tuning these hyperparameters since this will be directly reflected in the predictive accuracy of the model and the generalization capability on new data. Such a procedure helps researchers in fine-tuning the models according to their datasets, hence their reliability and efficiency in different applications.

Table 3 The hyperparameters results for hybrid models of DTC

Models	Hyperparameter		
	Max_depth	Min_samples_split	Min_samples_leaf
DTMO	8	0.8	0.19
DTFF	28	0.9	0.3

Table 4 The hyperparameters results for hybrid models of ELM

Models	Hyperparameter		
	Alpha	Batch_size	Density
ELMO	0.21	790	0.29
ELFF	0.6	2500	0.34

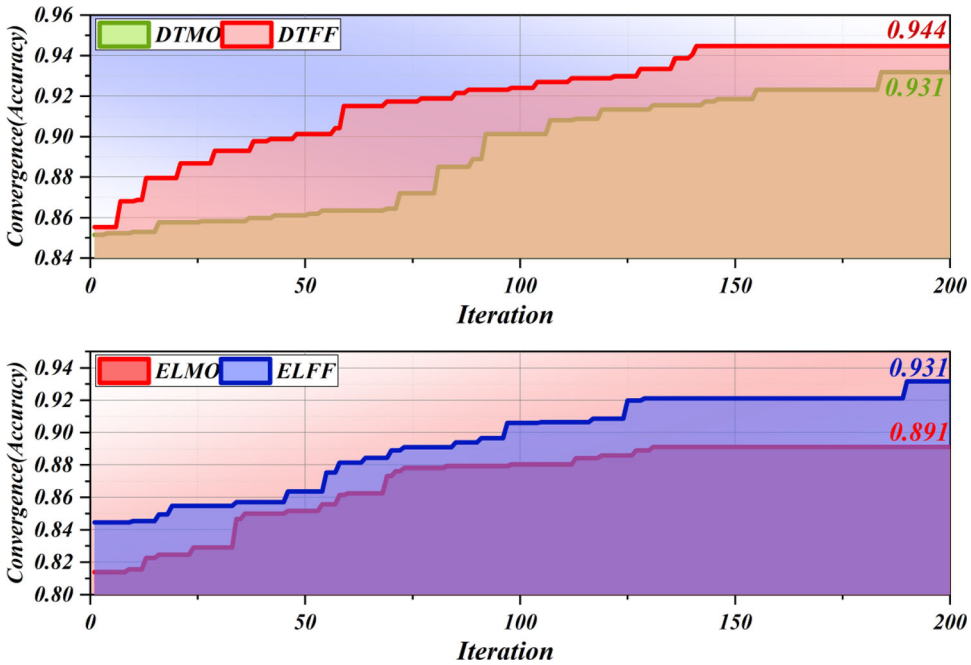

Fig. 4 The convergence curve of the ELM and DTC base hybrid models

3.2 Convergence curve

The convergence curve is useful because it may illustrate the advancement of a prediction procedure. As data repetitions occur, the curve graphically displays the convergence or divergence of forecast outcomes as they approach a stable solution. It functions as a diagnostic tool, revealing the model's convergence to optimal prediction performance or flagging possible problems such as overfitting or underestimating. Trends and patterns in the curve direct modifications to model parameters or algorithms, allowing for refinement and improvement in prediction accuracy without the need for active involvement. Figure 4 displays and compares the results of the DTMO, DTFF, ELMO, and ELFF models through convergence curves. Subsequently, the subsequent figure illustrates that between the DTMO and DTFF models, the DTMO model initiates the iteration process with an accuracy of 0.85. By the 100th iteration, this model's accuracy increases to 0.9. However, by the 150th iteration, the current model has reached its optimal condition, achieving an accuracy of 0.931. Conversely, the DTFF model underwent a gradual increase in accuracy through step-by-step refinement. For instance, before the 50th iteration, this model augmented its accuracy from 0.85 to 0.9, continuing to improve thereafter. Ultimately, before the 150th iteration, the model achieved its optimal condition, attaining an accuracy of 0.944. On the other hand, concerning the ELMO and ELFF models, the ELFF model demonstrates higher accuracy compared to the ELMO model. This model commences the iteration process with an accuracy of 0.84 and achieves an accuracy of 0.931 by approximately the 130th iteration, showcasing superior performance relative to the ELMO model, which achieves an accuracy of 891 by the 140th iteration.

3.3 Models comparison based on evaluation metrics

Table 5 displays the outcomes of the developed models across 3 phases: Train, Test, and All. As indicated, among the DTC model and its hybrid variants, the highest accuracy is attributed to the DTFF model throughout the testing phase, with an accuracy of 0.951, followed by the DTMO model with 0.932 accuracy, surpassing the DTC model's accuracy of 0.918. The lowest outcomes are attributed to the ELM model. For instance, the ELM model exhibits the weakest performance in this comparison, with an accuracy of 0.824. Although the ELMO model demonstrates improved performance over the base model with an accuracy of 0.894, it still falls short in functionality compared to the ELFF model, which achieves an accuracy of 0.944 in the training phase.

Figure 5 offers a comprehensive depiction of the models' outcomes across 3 distinct phases, utilizing a line plot for visual clarity. During the testing phase, the DTC model showcases its robust functionality, boasting a precision metric value of 0.927. Similarly, the ELM model demonstrates comparable performance, with a precision value of 0.863 in the same phase, reflecting its efficacy in training. Transitioning to the testing phase, the DTMO model emerges as the frontrunner, achieving the highest F1-score value of 0.932, signifying its exceptional predictive capability. Meanwhile, the DTFF model exhibits consistent superiority across all

Table 5 The outcome of the showcased developed models

Section	Model	Metric values				
		Accuracy	Precision	Recall	F1-score	MCC
Train	DTC	0.860	0.897	0.860	0.862	0.753
	DTMO	0.932	0.933	0.932	0.932	0.859
	DTFF	0.943	0.944	0.943	0.943	0.882
	ELM	0.824	0.842	0.824	0.826	0.657
	ELMO	0.891	0.895	0.891	0.892	0.778
	ELFF	0.929	0.930	0.929	0.929	0.853
Test	DTC	0.918	0.927	0.918	0.914	0.821
	DTMO	0.932	0.934	0.932	0.933	0.852
	DTFF	0.951	0.951	0.951	0.951	0.892
	ELM	0.863	0.863	0.863	0.863	0.695
	ELMO	0.894	0.897	0.894	0.895	0.770
	ELFF	0.944	0.946	0.944	0.945	0.879
All	DTC	0.872	0.900	0.872	0.871	0.772
	DTMO	0.932	0.932	0.932	0.932	0.862
	DTFF	0.945	0.945	0.945	0.945	0.889
	ELM	0.832	0.842	0.832	0.832	0.672
	ELMO	0.892	0.893	0.892	0.892	0.783
	ELFF	0.932	0.932	0.932	0.932	0.863

metrics, highlighting its exceptional performance comprehensively.

Table 6 displays and compares the models' performance under two conditions, namely Non-Tumor and Tumor conditions. In the Non-Tumor condition, the DTC model exhibits a precision value of 1, which represents the highest among all models. Subsequently, the DTMO model achieves a precision value of 0.948, indicating inferior functionality compared to the DTFF model, which boasts a precision value of 0.958 under the same condition. However, the highest precision value among the ELM model and its hybrid forms is attributed to the ELFF model, with a precision value of 0.949, which is lower than the precision values of the DTFF model and DTMO models. Furthermore, the ELMO model, with a precision value of 0.917, demonstrates superior functionality compared to the ELM model, which achieves a precision value of 0.901 under the same condition.

Under the tumor condition, the lowest recall values are attributed to DTC, ELM, and ELMO, with recall values of 0.768, 0.781, and 0.884, respectively. Conversely, DTFF, DTMO, and ELFF models exhibit higher recall values of 0.941, 0.927, and 0.926, respectively, thereby demonstrating their superior functionality compared to the former models.

In this comparison, it is observed that most of the time when the base models are combined with FFO, their accuracy surpasses that of other models. By comparing the F1-score values of the ELFF and DTFF models under both non-tumor and tumor conditions, it is evident that the DTFF model outperforms the ELFF model. Specifically, under the non-tumor condition, the DTFF model achieves an F1-score value of 0.949, whereas the ELFF model attains a lower value of 0.938. Similarly, under the tumor condition, the ELFF model records an F1-score value of 0.924, indicating inferior performance compared to the DTFF model, which achieves a higher F1-score value of 0.938.

Figure 6 compares the predicted values of the presented models based on the measured values under both tumor and non-tumor conditions using a line symbol plot. As observed, among the DTC, DTMO, and DTFF models, under the non-tumor condition, the DTFF model, with 1956 out of 2079 measured values, demonstrates the highest functionality in the prediction process. Following this, the DTMO model, with 1928 out of 2079 measured values, indicates intermediate functionality among the DTFF and DTC models, which record 1596 out of 2079 measured values. Similarly, under the tumor condition, the ETFF model's performance surpasses that of the other models. On the other side, among the ELM, ELMO, and ELFF models, the accuracy of the ELMO model exceeds that of the ELM model, with 1505 out of 1683 measured values, and falls short of the ELFF model, which achieves 1579 out of 1683 measured values. Under the nontumor condition, the highest accuracy is attributed to the ELFF model, with 1926 out of 2079 measured values.

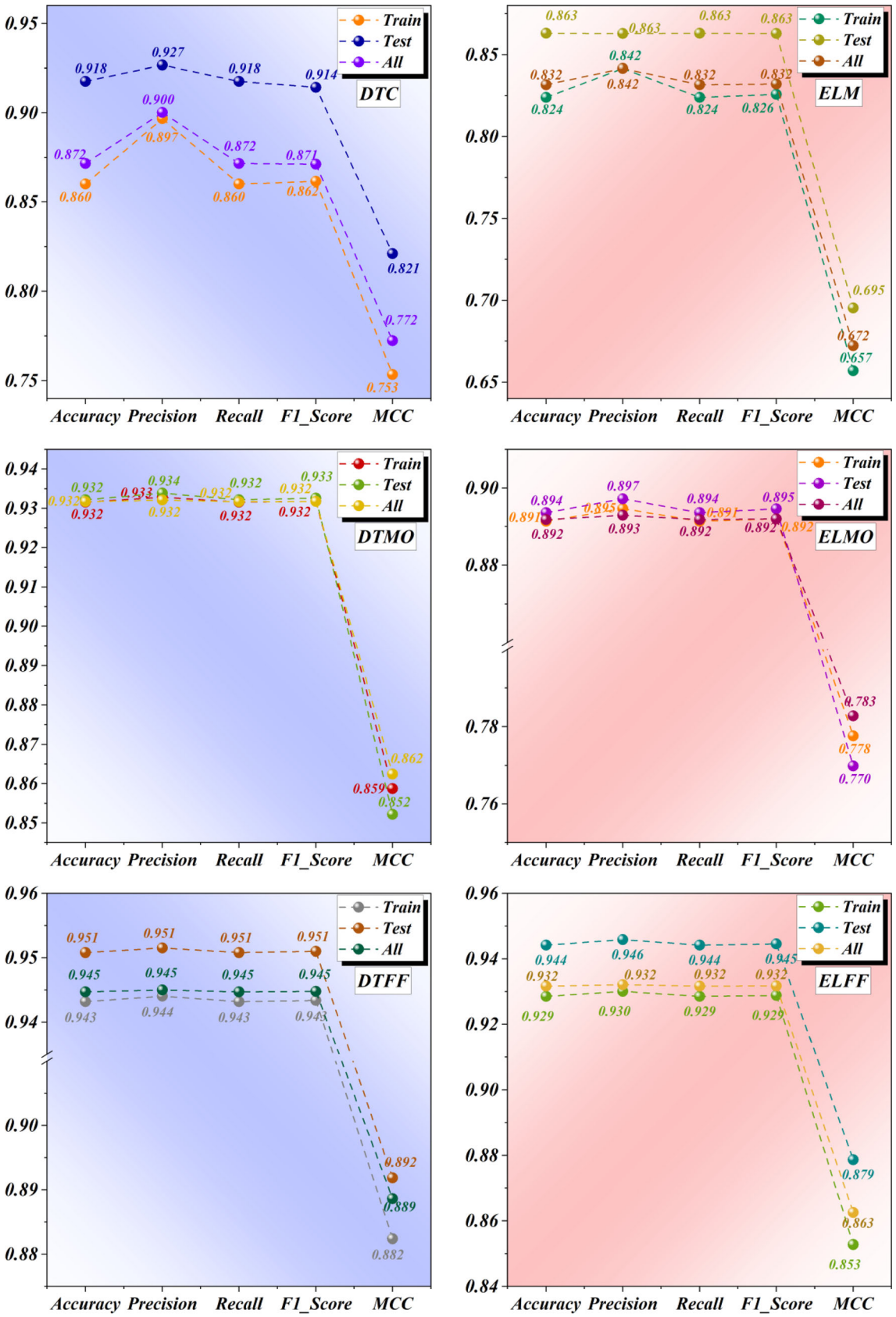

Fig. 5 The line-symbol plot for the performance of the models

Table 6 Categorization of assessment criteria regarding the functionality of the created models

Metric values	Condition	Model					
		DTC	DTMO	DTFF	ELM	ELMO	ELFF
Precision	Non-tumor	1	0.948	0.958	0.901	0.917	0.949
	Tumor	0.777	0.913	0.928	0.767	0.863	0.912
Recall	Non-tumor	0.768	0.927	0.941	0.781	0.884	0.926
	Tumor	1	0.937	0.949	0.894	0.902	0.938
F1-score	Non-tumor	0.869	0.937	0.949	0.837	0.900	0.938
	Tumor	0.875	0.925	0.938	0.826	0.882	0.924

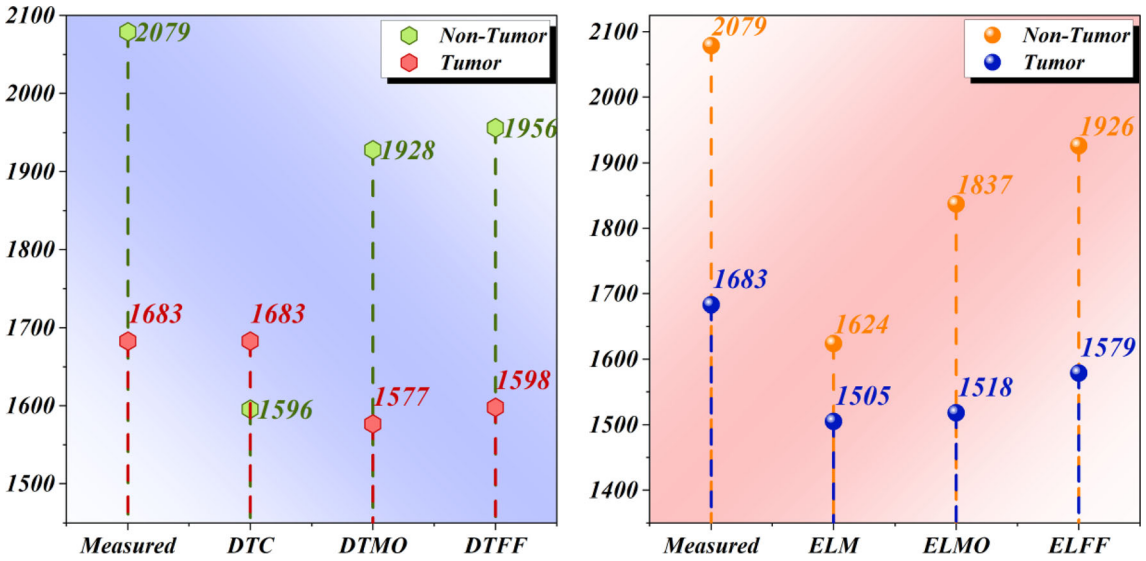

Fig. 6 Models predicted and measured values

Subsequently, the ELMO model, with 1837 out of 2079 measured values, demonstrates superior functionality compared to the ELM model, which records 1624 out of 2079 measured values.

3.4 Wilcoxon test

To assess the comparative performance of six models—DTC, DTMO, DTFF, ELM, ELMO, and ELFF—the Wilcoxon test was employed. Detailed results of the test, including p-values and test statistics for each model pair, are summarized in Table 7, offering insights into their statistical significance. The analysis indicates no statistically significant differences between the performance of DTMO and DTFF (p-value = 0.734795, Statistic = 44,940), DTMO and ELFF (p-value = 0.853923, Statistic = 55,341), or DTFF and ELFF (p-value = 0.598748, Statistic = 46,647). Notably, the comparison between DTC and DTFF shows a marginally significant difference (p-value = 9.76E−69, Statistic = 32,300). Although this difference does not fully meet conventional significance levels, it suggests a potential area for further investigation.

Table 7 Result of Wilcoxon test

Difference of models	Parameter	
	P-value	Statistic
Def. between DTC and DTMO	8.54E−65	37,572.5
Def. between DTC and DTFF	9.76E−69	32,300
Def. between DTC and ELM	6.23E−12	155,527
Def. between DTC and ELMO	7.05E−48	73,023.5
Def. between DTC and ELFF	5.03E−64	37,346.5
Def. between DTMO and DTFF	0.734795	44,940
Def. between DTMO and ELM	2.16E−16	113,058.5
Def. between DTMO and ELMO	0.19874	91,287
Def. between DTMO and ELFF	0.853923	55,341
Def. between DTFF and ELM	9.07E−18	103,984
Def. between DTFF and ELMO	0.10326	76,629
Def. between DTFF and ELFF	0.598748	46,647
Def. between ELM and ELMO	4.88E−12	133,820.5
Def. between ELM and ELFF	1.05E−15	117,305
Def. between ELMO and ELFF	0.258481	90,097.5

In conclusion, while DTMO and DTFF, as well as DTMO and ELFF pairs, demonstrate similar performance, the DTC and DTFF pair may require additional examination due to the observed marginal significance.

4 Discussion

4.1 Limitation of the study

1. *Data quality and availability* The accuracy of the predictive models heavily depends on the quality and quantity of the dataset used. Limitations in data size, diversity, and the availability of high-quality labeled data may have influenced the model's performance and generalizability.
2. *Lack of real-world validation* While the models were tested using existing datasets, they may not have been validated with diverse clinical data or real-world patient populations. This gap highlights the need for external validation to confirm the models' reliability in varied healthcare environments.
3. *Interpretability of ML MODELS* Although Decision Tree models tend to be more interpretable, the use of advanced optimization techniques may still obscure the reasoning behind certain predictions, making it difficult for medical practitioners to understand how decisions are derived.

4.2 Practical implications

1. *Enhanced brain tumor prediction* The study's findings demonstrate that ML models, particularly those optimized with advanced algorithms (the FFO and MO), significantly improve the accuracy of brain tumor predictions. This can help clinicians make more informed and timely decisions regarding diagnosis and treatment.
2. *Model integration in clinical decision-making* The superior performance of DTC-based models, particularly the DTFF model, suggests that these techniques could be integrated into diagnostic tools to assist radiologists and medical professionals in identifying tumor characteristics more accurately, potentially leading to personalized treatment strategies.
3. *Optimization techniques in medical data analysis* By leveraging optimization techniques to refine ML model performance, the study highlights the importance of combining optimization algorithms with predictive models to handle complex medical datasets. This approach could be applied to other areas of medical diagnostics beyond brain tumor prediction.
4. *Reduction of diagnostic errors* The improved precision of hybrid models may reduce false positives and false negatives in brain tumor diagnoses, leading to better patient outcomes by ensuring that only those in need receive aggressive treatments, while others avoid unnecessary procedures.

4.3 Potential future studies

1. *Real-world clinical trials* Future research should involve validating these hybrid models with larger, more diverse patient datasets from multiple healthcare institutions to ensure they generalize well across different populations and clinical environments.
2. *Integration with multimodal data* Incorporating other data types, such as genetic profiles, biomarkers, patient history, and neuroimaging data, could improve the models' predictive capabilities and lead to more comprehensive diagnostic tools for brain tumor detection and classification.
3. *Exploration of new optimization algorithms* Investigating the use of other cutting-edge optimization techniques or developing new algorithms could further refine the accuracy and efficiency of ML models for medical applications.
4. *Real-time monitoring systems* Developing AI-powered systems that use these models to monitor patients in real-time could help track tumor progression and provide insights into treatment effectiveness, ultimately leading to more dynamic and adaptive treatment plans.
5. *Explainable AI in healthcare* Future studies could focus on improving the interpretability and transparency of these predictive models, ensuring that healthcare professionals can clearly understand the factors driving the predictions, thus facilitating their acceptance in clinical practice.
6. *Hybrid models in other medical conditions* Extending the research to include hybrid ML models optimized with advanced algorithms for predicting other types of cancers or neurological disorders could open new avenues for AI-driven diagnostics in the broader medical field.

5 Conclusion

A brain tumor is characterized by the abnormal growth of cells within the structures of the brain or its contiguous tissues. They are benign or malignant, and in addition, may arise from various types of brain tissue or from extra-cerebral tissues that have spread to the brain. Symptoms include

headaches, seizures, cognitive deficits, and changes in behavior or personality, all of which vary with the location and size of the tumor. Imaging studies like MRI or CT scans are often utilized to make a diagnosis, which is then confirmed by a biopsy. Surgery, radiation treatment, treatment with chemotherapy, or an amalgamation of the 3 may be used to treat the tumor, depending on its features and the patient's general condition. Brain tumor prediction is sought through Machine Learning (ML) models, specifically Extreme Learning Model (ELM) and Decision Tree Classification (DTC), along with two optimizers, namely Flying Fox Optimizer (FFO) and Mayfly Optimizer (MO). To enhance prediction accuracy, the decision was made to combine these models with optimizers, resulting in the creation of new hybrid models. Considering the results, it can be concluded that:

- The results indicate that within the groups of DTC-based and ELM-based models, the DTC-based models demonstrate superior performance in both tumor and nontumor conditions compared to the ELM model and its hybrid variations.
- In the context of tumor conditions, the DTFF model demonstrates superior capability with a precision value of 0.932, surpassing the precision values of DTMO and DTC, which stand at 0.904 and 0.856, respectively.
- Comparing the results of DTC-based and ELM-based models, the outcomes of DTFF and DTMO generally outperform those of the ELFF model (0.913), ELMO (0.877), and the ELM model (0.804) under the same conditions.

Acknowledgements We would like to take this opportunity to acknowledge that there are no individuals or organizations that require acknowledgment for their contributions to this work.

Author contributions ZD: Writing-original draft preparation, conceptualization, supervision, project administration.

Funding This work was supported by the Key Scientific Research Foundation of Hunan Provincial Department of Education (no. 23A0575); in part by the Hunan Provincial Natural Science Foundation (nos. 2024JJ7184, 2024JJ7187); in part by the Project of Hunan Provincial Social Science Achievement Review Committee in 2023 (no. XSP2023JYC283); in part by the Science Communication Research and Practice Project of Hunan Association for Science and Technology in 2023 (no. 2023jckpkt096) and in part by the General Research Projects of Hunan Provincial Department of Education (no. 23C0358).

Availability of data and materials No datasets were generated or analysed during the current study.

Declarations

Conflict of interest The authors declare no competing interests.

References

Aalloul R, Elaissaoui A, Benlattar M, Adhiri R (2023) Emerging parameters extraction method of pv modules based on the survival strategies of flying foxes optimization (FFO). Energies 16:3531

Abd-Ellah MK, Awad AI, Khalaf AAM, Hamed HFA (2019) A review on brain tumor diagnosis from MRI images: practical implications, key achievements, and lessons learned. Magn Reson Imaging 61:300–318

Alzubi JA, Kumar A, Alzubi O, Manikandan R (2019) Efficient approaches for prediction of brain tumor using machine learning techniques. Indian J Public Heal Res Dev 10:237

Amudha M, Ramachandran M, Sivaji C, Gayathri R (2021) A study on climate change with mayfly algorithm optimization. Recent Trends Manag Commer 2:23–28

Bakas S, Reyes M, Jakab A, Bauer S, Rempfler M, Crimi A et al (2018) Identifying the best machine learning algorithms for brain tumor segmentation, progression assessment, and overall survival prediction in the BRATS challenge. ArXiv 181102629.

Batta A (2017) Increasing incidence of brain tumors. Int J Curr Res Med Sci 3:13–21

Bauer R, Ortler M, Seiz-Rosenhagen M, Maier R, Anton JV, Unterberger I (2014) Treatment of epileptic seizures in brain tumors: a critical review. Neurosurg Rev 37:381–388

Brain Tumor Data n.d. https://www.kaggle.com/datasets/jakeshbohaju/brain-tumor.

Cacho-Díaz B, García-Botello DR, Wegman-Ostrosky T, Reyes-Soto G, Ortiz-Sánchez E, Herrera-Montalvo LA (2020) Tumor microenvironment differences between primary tumor and brain metastases. J Transl Med 18:1–12

Cao J, Lin Z, Huang G-B (2012) Self-adaptive evolutionary extreme learning machine. Neural Process Lett 36:285–305

Dolecek TA, Propp JM, Stroup NE, Kruchko C (2012) CBTRUS statistical report: primary brain and central nervous system tumors diagnosed in the United States in 2005–2009. Neuro Oncol 14:v1-49

Durand T, Berzero G, Bompaire F, Hoffmann S, Léger I, Jego V et al (2018) Episodic memory impairments in primary brain tumor patients. Arch Clin Neuropsychol 33:949–955

Ghandour F, Squassina A, Karaky R, Diab-Assaf M, Fadda P, Pisanu C (2021) Presenting psychiatric and neurological symptoms and signs of brain tumors before diagnosis: a systematic review. Brain Sci 11:301

Gordon P, LeGrand SB, Walsh D (2014) Nausea and vomiting in advanced cancer. Eur J Pharmacol 722:187–191

Hadidchi S, Surento W, Lerner A, Liu CSJ, Gibbs WN, Kim PE et al (2019) Headache and brain tumor. Neuroimaging Clin 29:291–300

Huang G-B, Zhu Q-Y, Siew C-K (2006) Extreme learning machine: theory and applications. Neurocomputing 70:489–501

Huang G-B, Zhou H, Ding X, Zhang R (2011) Extreme learning machine for regression and multiclass classification. IEEE Trans Syst Man Cybern Part B 42:513–529

Kumar S, Tejani GG, Pholdee N, Bureerat S (2021) Multiobjecitve structural optimization using improved heat transfer search. Knowledge-Based Syst 219:106811

Lemaitre A-L, Herbet G, Duffau H, Lafargue G (2021) Personality and behavioral changes after brain tumor resection: a lesion mapping study. Acta Neurochir (Wien) 163:1257–1267

Li Y, Lu W, Pan Z, Wang Z, Dong G (2023) Simultaneous identification of groundwater contaminant source and hydraulic parameters based on multilayer perceptron and flying foxes optimization. Environ Sci Pollut Res 30:1–15

Liu Z, Jiang P, Wang J, Zhang L (2021) Ensemble forecasting system for short-term wind speed forecasting based on optimal sub-model

selection and multi-objective version of mayfly optimization algorithm. Expert Syst Appl 177:114974
Naji K (2018) Resilient modulus–moisture content relationships for pavement engineering applications. Int J Pavement Eng 19:651–660
Olson S, Law A (2005) Meningiomas and the Polynesian population. ANZ J Surg 75:705–709
Pal M, Deswal S (2014) Extreme learning machine based modeling of resilient modulus of subgrade soils. Geotech Geol Eng 32:287–296
Park JH, de Lomana ALG, Marzese DM, Juarez T, Feroze A, Hothi P et al (2021) A systems approach to brain tumor treatment. Cancers (Basel) 13:3152
Pekmezci M, Perry A (2013) Neuropathology of brain metastases. Surg Neurol Int 4:S245
Priya KM, Kavitha S, Bharathi B, Brain tumor types and grades classification based on statistical feature set using support vector machine. (2016) 10th Int. Conf. Intell. Syst. Control. IEEE 2016:1–8
Robert-Boire V, Desnous B, Lortie A, Carmant L, Ellezam B, Weil AG et al (2019) Seizures in pediatric patients with primary brain tumors. Pediatr Neurol 97:50–55
Shankar GM, Balaj L, Stott SL, Nahed B, Carter BS (2017) Liquid biopsy for brain tumors. Expert Rev Mol Diagn 17:943–947
Sudha B, Gopikannan P, Shenbagarajan A, Balasubramanian C (2014) Classification of brain tumor grades using neural network. Proc World Congr Eng 1:2–4
Thust SC, van den Bent MJ, Smits M (2018) Pseudoprogression of brain tumors. J Magn Reson Imaging 48:571–589
Woroniecka K, Chongsathidkiet P, Rhodin K, Kemeny H, Dechant C, Farber SH et al (2018) T-cell exhaustion signatures vary with tumor type and are severe in glioblastoma. Clin Cancer Res 24:4175–4186
Wrensch M, Minn Y, Chew T, Bondy M, Berger MS (2002) Epidemiology of primary brain tumors: current concepts and review of the literature. Neuro Oncol 4:278–299
Zhou M, Scott J, Chaudhury B, Hall L, Goldgof D, Yeom KW et al (2018) Radiomics in brain tumor: image assessment, quantitative feature descriptors, and machine-learning approaches. Am J Neuroradiol 39:208–216